J. Meas. Sci. Instrum., 2024, 15(3): 302-307. http://jmsi.publish.founderss.cn
DOI: 10.62756/jmsi.1674-8042.2024031 jmsi@nuc.edu.cn

Construction of a broadband impedance spectrum and synchronous DC voltammetry measurement system for solar cells

XIAO Wenbo[1,2,3*], LI Ao[2], WU Huaming[2], LI Yongbo[2]

1.College of Science and Technology, Nanchang Hangkong University, Jiujiang 332020, China;
2.Key Laboratory for Optoelectronic Information Perception and Instrumentation of Jiangxi Province, Nanchang Hangkong University, Nanchang 330063, China;
3. Key Laboratory of Nondestructive Testing of Ministry of Education, Nanchang Hangkong University, Nanchang 330063, China

***Corresponding author:** XIAO Wenbo (xiaowenbo1570@163.com)

Received: March 26, 2024 **Revised:** April 21, 2024 **Accepted:** May 3, 2024

Abstract: The current impedance spectroscopy measurement techniques face difficulties in diagnosing solar cell faults due to issues such as cost, complexity, and accuracy. Therefore, a novel system was developed for precise broadband impedance spectrum measurement of solar cells, which was composed of an oscilloscope, a signal generator, and a sampling resistor. The results demonstrate concurrent accurate measurement of the impedance spectrum (50 Hz—0.1 MHz) and direct current voltametric characteristics. Comparative analysis with Keithley 2450 data yields a global relative error of approximately 6.70%, affirming the accuracy. Among excitation signals (sine, square, triangle, pulse waves), sine wave input yields the most accurate data, with a root mean square error of approximately 13.301 6 and a global relative error of approximately 4.25% compared to theoretical data. Elevating reference resistance expands the half circle in the impedance spectrum. Proximity of reference resistance to that of the solar cell enhances the accuracy by mitigating line resistance influence. Measurement error is lower in high-frequency regions due to a higher signal-to-noise ratio.

Key words: solar cell; oscilloscope; signal generator; volt-ampere characteristics; impedance spectrum

0 Introduction

Photovoltaic (PV) power generation is a widely used method of converting light energy into electricity, offering a promising solution to issues such as the depletion of fossil fuels[1-3]. However, PV power generation can be unreliable due to fluctuations in the working environment, and cell failures can also affect its power generation efficiency[4-7]. Therefore, impedance measurement for characterizing the dynamic performance of solar cells and analyzing their working mechanism has gradually become a focus of attention[8-11]. The reason is that the impedance spectrum contains not only direct current (DC) resistance information, but also dynamic capacitance, inductance, and other internal information[12-14].

The impedance measurement principle involves applying a small excitation signal to the tested object and analyzing the corresponding response signal in terms of phase, amplitude, and frequency. Typically, this information is represented using a Nyquist diagram[15]. Currently, impedance spectra are obtained through the use of electrochemical workstations[16] or microcontroller embedded systems[17]. By comparisen, electrochemical workstations offer high measurement accuracy, but they are expensive; the AD5933 chip microcontroller provides a more affordable alternative, but it has a limited frequency range of operation (5 kHz—100 kHz)[18]. However, utilizing embedded technology for impedance measurement can be complex and challenging[19,20]. Furthermore, both of these systems are limited to impedance spectrum measurement and cannot capture the DC volt-ampere characteristics. These DC volt-ampere characteristics are essential for diagnosing solar cell faults such as shading[21-23].

To address the aforementioned issues, a novel system for measuring solar cell impedance has been developed. The system primarily comprises a DG1022 model signal generator and a GDS-1102A model oscilloscope. It enables synchronous measurement of impedance spectrum and DC volt-ampere characteristics. Furthermore, the study investigates the effects of excitation signal type and reference resistance on the measurement.

1 Solar cell model, impedance spectrum measurement principle, and measurement process

Solar cells are semiconductor devices that convert solar energy into electrical energy[24,25]. The equivalent models of solar cells are divided into DC models[26] and AC models[27]. The AC equivalent model of a solar cell is shown in Fig. 1(a), which consists of a series resistor R_s, a parallel capacitor C_p, and a parallel resistor R_p[28]. The presence of circuit elements such as capacitors and resistors imply that the type of AC signal and reference resistance can influence the measurement outcomes.

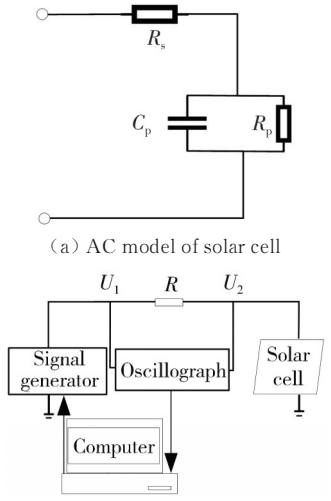

(a) AC model of solar cell

(b) System schematic

Fig. 1 Solar cell model and system principles

The schematic diagram is shown in Fig. 1(b). The input signal $\boldsymbol{U}_1$ represents the excitation signal generated by the signal generator, where R is the reference resistance, and the output signal $\boldsymbol{U}_2$ is the voltage signal across the impedance $\boldsymbol{Z}_x$ of the solar cell. According to Ohm's law, $\boldsymbol{Z}_x$ can be determined by

$$\boldsymbol{Z}_x = \frac{R\boldsymbol{U}_2}{\boldsymbol{U}_1 - \boldsymbol{U}_2}. \tag{1}$$

Suppose the amplitude and phase of $\boldsymbol{U}_1$ are A_1 and φ_1, respectively. And the amplitude and phase of $\boldsymbol{U}_2$ are A_2 and φ_2, respectively. The ratio is $\boldsymbol{X} = \boldsymbol{U}_2/\boldsymbol{U}_1$ and calculated in detailed by

$$\boldsymbol{X} = \frac{A_2 e^{j(\omega t+\varphi_2)}}{A_1 e^{j(\omega t+\varphi_1)}} = \frac{A_2}{A_1} e^{j(\varphi_2-\varphi_1)} = \frac{A_2}{A_1}\cos(\varphi_2-\varphi_1) + j\frac{A_2}{A_1}\sin(\varphi_2-\varphi_1). \tag{2}$$

By applying Eqs. (1) and (2), $\boldsymbol{Z}_x$ can be obtained as

$$\boldsymbol{Z}_x = \frac{R\boldsymbol{X}}{1-\boldsymbol{X}}. \tag{3}$$

The impedance spectrum obtained from a single measurement is shown in Fig. 2(a). This system can achieve measurements of 50 Hz to 0.1 MHz, and linear sampling is used in the monotonic region. Sampling points are appropriately added at the peak to make the impedance information more complete and smoother, compared with the impedance spectrum obtained in Refs. [29, 30]. Specifically, the system can capture low frequency information, which is typically missing in other measurement methods. Additionally, the measurements are performed uniformly across the frequency range, ensuring that the impedance spectrum is accurate and reliable.

In addition to measuring the impedance spectrum, the system can also measure the DC I-V curve. The system measures the DC I-V scatter of the solar cell, along with the curve obtained from the Keithley 2450, as depicted in Fig. 2 (b). The data measured by both methods exhibit negligible differences. The global relative error (GRE) between the two methods is calculated at approximately 6.70%, indicating the accuracy of the DC I-V characteristics measured using this approach.

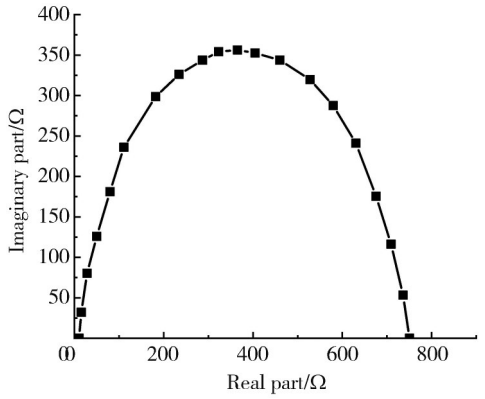

(a) Experimental results of impedance spectrum

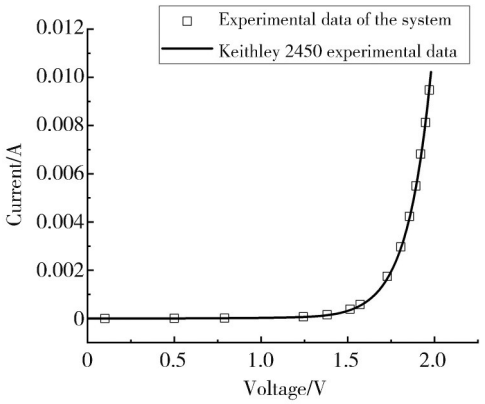

(b) Experimental results of I-V curve

Fig. 2 Experimental results of solar cell output characteristics

2 Factors affecting measurement results

2.1 Excitation signal type

Using sine, square, triangular, and pulse signals of the

same amplitude as excitation signals, the cell impedance was measured under dark condition. Then, error analysis was conducted on the experimental and theoretical fitting data. Root mean square error (RMSE) and GRE were used to assess the accuracy and reliability.

Fig.3 shows a comparison between experimental data and fitting curves. The red scatter data represent the experimental data obtained, and the blue square data and lines represent the fitting results. The experimental data are seen to be basically consistent with the theoretical fitting results, which means the measurement results are basically correct. RMSE and GRE, as well as those at high- and low- frequency regions (bounded by the central axis, with the left part being high- frequency region and the right part being low-frequency region), are shown in Table 1.

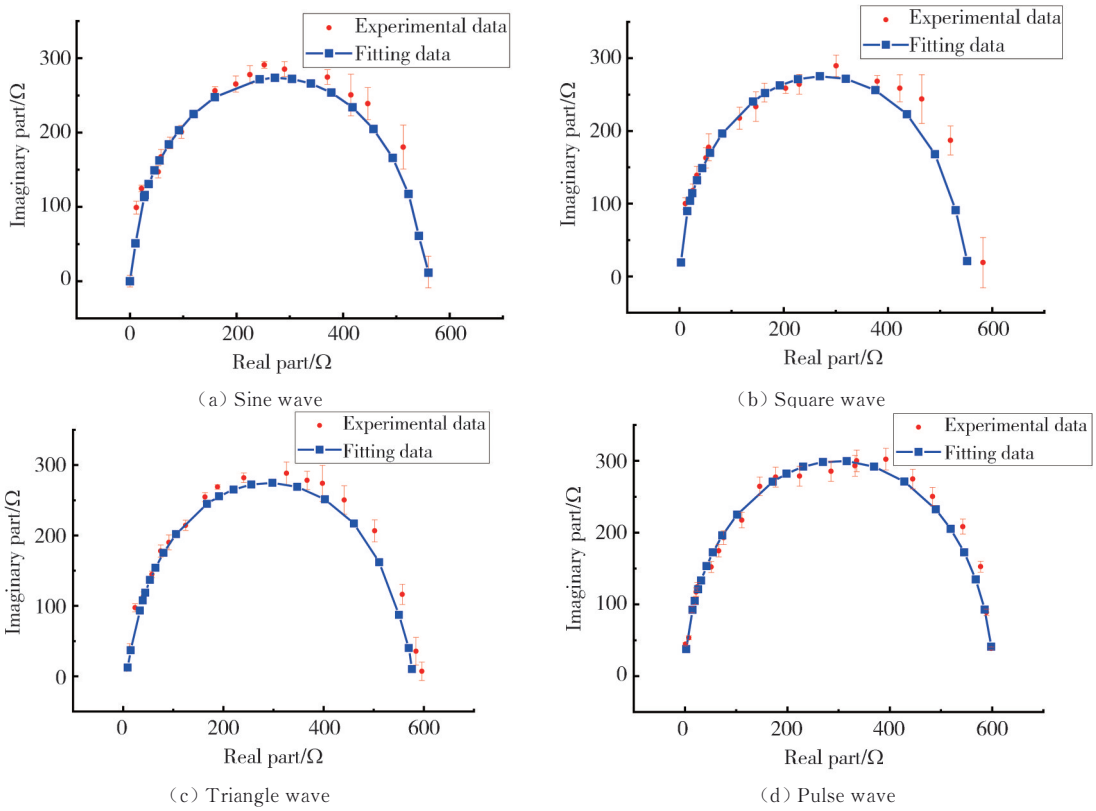

Fig. 3 Experimental results obtained at different excitation signals

Table 1 RMSE and GRE, as well as those at high- and low- frequency regions for different excitation signals

Excitation signal	RMSE	RMSE of low frequency	RMSE of high frequency	GRE/%	GRE of low frequency/%	GRE of high frequency/%
Sine wave	13.301 6	26.116 9	9.555 43	4.25	10.59	3.35
Square wave	24.351 2	43.808 1	11.775 8	8.26	17.82	5.75
Triangular wave	18.347 6	26.246 8	12.908 1	7.78	13.69	5.81
Pulse wave	14.515 9	21.891 3	8.397 57	6.04	9.02	4.64

When sine wave, square wave, triangular wave, and pulse wave signals are used as inputs, RMSE (GRE) approximately is 13.301 6 (4.25%), 24.351 2 (8.26%), 18.347 6(7.78%), and 14.515 9 (6.04%), respectively. The reason is that a square wave will cause more high-frequency response and be affected by harmonics. But a sine wave is less susceptible to interference and distortion. Therefore, the error is the smallest when a sine wave is used as the excitation signal. According to RMSE (GRE) of the high- and low- frequency regions in Table 1, both RMSE and GRE are found to be smaller in the high-frequency region than that in the low- frequency region. The reason may be 1) the signal generator easily generates nonlinear errors in the low- frequency region, such as distortion, offset, etc; and 2) the signal-to-noise ratio in the low-frequency region is relatively weak and more susceptible to noise interference.

2.2 Reference resistance

Impedance spectrum were got by using reference resistances of 90 Ω, 240 Ω, 400 Ω, and 500 Ω, respectively. The results are shown in Fig.4, with scattered red dots representing experimental data and the blue square data and lines representing the fitting results. The experiment data are seen to be basically consistent with the theoretical fitting

results, which also indicates the correctness of the measurement results. In addition, it is noted that the impedance spectrum semicircle increases with the increase of the reference resistance value. The reason is that the value of reference resistance increases, which is equivalent to increasing the series resistance of the circuit.

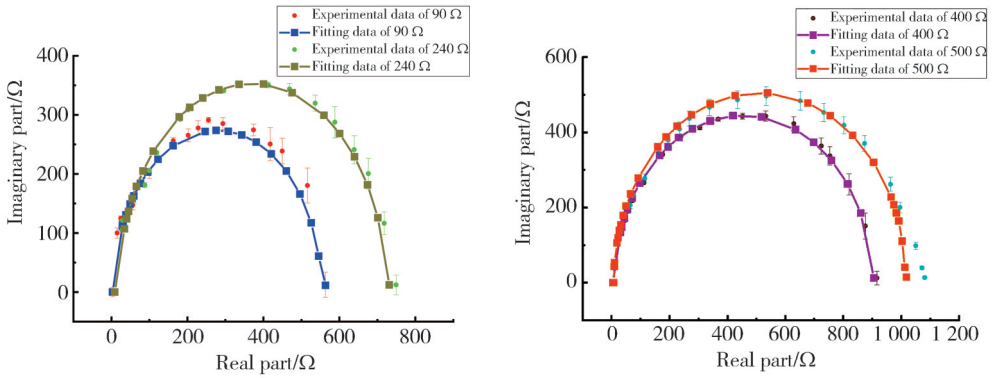

(a) Reference resistances of 90 Ω and 240 Ω (b) Reference resistances of 400 Ω and 500 Ω

Fig. 4 Experimental results obtained at different reference resistances

RMSE and GRE, as well as those at high- and low-frequency regions at reference resistances of 90 Ω, 240 Ω, 400 Ω, and 500 Ω are shown in Table 2. RMSE and GRE are found to be the smallest (10.953 93 and 3.84%) when the reference resistance value is 400 Ω. The closer the reference resistance is to the internal resistance of the battery, the less the influence of line resistance in the circuit can be reduced. The internal resistance of the solar cell is approximately 430 Ω, so the highest accuracy is obtained when selecting a reference resistance of 400 Ω. In addition, it is observed that RMSE or GRE in the high-frequency region is also lower than that in the low-frequency region, which is consistent with the above conclusion.

Table 2 RMSE and GRE, as well as those at high- and low-frequency regions at reference resistances of 90 Ω, 240 Ω, 400 Ω, and 500 Ω

Reference resistor/Ω	RMSE	RMSE of low frequency	RMSE of high frequency	GRE/%	GRE of low frequency/%	GRE of high frequency/%
90	17.087 91	26.116 86	9.555 432	5.80	10.60	3.35
240	16.517 86	19.334 27	15.258 61	7.50	8.50	5.46
400	10.953 93	12.473 16	9.917 94	3.84	4.23	3.92
500	14.341 13	19.222 03	12.340 46	4.87	5.55	4.81

3 Conclusions

In our work, a system has been developed to accurately measure the broadband impedance spectrum of solar cells. The key hardware components include an oscilloscope, a signal generator, and a sampling resistor. The following results have been achieved. The system enables impedance spectrum measurement in the frequency range of 50 Hz to 0.1 MHz It allows simultaneous measurement of DC volt-ampere characteristics, yielding a global relative error of approximately 6.70% compared to measurements obtained from the Keithley 2450 source meter. This demonstrates the accuracy of the system. The study highlights the impact of the excitation signal choice on the measurement results. Among the tested excitations signals (sine, square, triangle, and pulse waves), the sine wave signal produces the most accurate experimental data. Its RMSE is approximately 13.3016, with a global relative error approximately of 4.25% compared to theoretical simulation data. This is attributed to the lower susceptibility of sine wave signal to interference and distortion, leading to more precise measurements. The size of the half circle in the impedance spectrum increases as the reference resistance is raised. This phenomenon can be attributed to the corresponding rise in series resistance within the circuit caused by the larger reference resistance. The measurement results are more precise when the reference resistance and the solar cell resistance are similar to each other. The measurement error in the high-frequency region is smaller than that in the low-frequency region, mainly due to a higher signal-to-noise ratio.

Acknowledgement

This work was financially supported by National Natural Science Foundation of China (Nos. 12064027, 62065014, 12464010); 2022 Jiangxi Province High-level and High-skilled Leading Talent Training Project

Selected (No. 63), Jiujiang "Xuncheng Talents" (No. JJXC2023032), Nanchang Hangkong University Education Reform Project (No.JY21069).

Declaration of conflicting interests

On behalf of all authors, the corresponding author states that there is no conflict of interest.

References

[1] LI J, ZHENG D Y. Short-term photovoltaic power prediction using combined K-SVD-OMP and KELM method. Journal of Measurement Science and Instrumentation, 2022, 13(3): 320-328.

[2] MAGHRABIE H M, ELSAID K, SAYED E T, et al. Phase change materials based on nanoparticles for enhancing the performance of solar photovoltaic panels: A review. Journal of Energy Storage, 2022, 48: 103937.

[3] DHASS A, BEEMKUMAR N, HARIKRISHNAN S, et al. A review on factors influencing the mismatch losses in solar photovoltaic system. International Journal of Photoenergy, 2022, 2022: 2986004.

[4] ZHOU H X, ZHANG Y J, YANG L F, et al. Short-term photovoltaic power forecasting based on long short-term memory neural network and attention mechanism. IEEE Access, 2019, 7: 78063-78074.

[5] AGGA A, ABBOU A, LABBADI M, et al. CNN-LSTM: An efficient hybrid deep learning architecture for predicting short-term photovoltaic power production. Electric Power Systems Research, 2022, 208: 107908.

[6] WANG X Y, SUN Y L, LUO D, et al. Comparative study of machine learning approaches for predicting short-term photovoltaic power output based on weather type classification. Energy, 2022, 240: 122733.

[7] LIU D, LIU Y M, SUN K. Policy impact of cancellation of wind and photovoltaic subsidy on power generation companies in China. Renewable Energy, 2021, 177: 134-147.

[8] KUIPERS M, SCHRÖER P, NEMETH T, et al. An algorithm for an online electrochemical impedance spectroscopy and battery parameter estimation: Development, verification and validation. Journal of Energy Storage, 2020, 30: 101517.

[9] VON HAUFF E. Impedance spectroscopy for emerging photovoltaics. The Journal of Physical Chemistry C, 2019, 123(18): 11329-11346.

[10] VON HAUFF E, KLOTZ D. Impedance spectroscopy for perovskite solar cells: characterisation, analysis, and diagnosis. Journal of Materials Chemistry C, 2022, 10(2): 742-761.

[11] MAKHLOUF M M, KHALLAF H, SHEHATA M M. Impedance spectroscopy and transport mechanism of molybdenum oxide thin films for silicon heterojunction solar cell application. Applied Physics A, 2022, 128(2): 98.

[12] DE BEER D J, JOUBERT T H. Under sampling and saturation for impedance spectroscopy performance. IEEE Sensors Journal, 2021, 21(20): 23382-23389.

[13] JONES P K, STIMMING U, LEE A A. Impedance-based forecasting of lithium-ion battery performance amid uneven usage. Nature Communications, 2022, 13(1): 4806.

[14] ASTAFEV E. Electrochemical noise measurement of a lithium iron (II) phosphate ($LiFePO_4$) rechargeable battery. Instrumentation Science & Technology, 2020, 48(1), 75-85.

[15] DE ANGELIS A, BUCHICCHIO E, SANTONI F, et al. Uncertainty characterization of a practical system for broadband measurement of battery EIS. IEEE Transactions on Instrumentation and Measurement, 2022, 71: 1002609.

[16] LIE S, BRUNO A, WONG L H, et al. Semitransparent perovskite solar cells with >13% efficiency and 27% transparency using plasmonic Au nanorods. ACS Applied Materials & Interfaces, 2022, 14(9): 11339-11349.

[17] LI M, NIAN H, HU B, et al. An improved impedance measurement method based on multi-sine signal considering the suppression of noise interference. IEEE Access, 2021, 9: 34221-34230.

[18] SIMIĆ M. Complex impedance measurement system for the frequency range from 5 kHz to 100 kHz. Key Engineering Materials, 2015, 644: 133-136.

[19] GAO S, LV R H, SUN S J. A Novel Touch interface with ultrahigh optical transmittance based on electrical impedance tomography for interactive displays. Advanced Materials Technologies, 2022, 7(6): 2101133.

[20] RANGKUTI H, SINAGA N, ARIANI F. Solar tracker design on solar panel for stm32 microcontroller based on battery charging system//4th International Conference on Natural Resources and Technology, August 29-30, 2022, Sumatera Utara, Indonesia. IOP Conference Series: Earth and Environmental Science, 2022, 1115(1): 012078.

[21] ZHANG Z H, MA M P, WANG H, et al. A fault diagnosis method for photovoltaic module current mismatch based on numerical analysis and statistics. Solar Energy, 2021, 225: 221-236.

[22] SARIKH S, RAOUFI M, BENNOUNA A, et al. Fault diagnosis in a photovoltaic system through I-V characteristics analysis//2018 9th International Renewable Energy Congress, March 20-22, 2018, Hammamet, Tunisia. New York: IEEE, 2018: 1-6.

[23] DHANRAJ J A, MOSTAFAEIPOUR A, VELMURUGAN K, et al. An effective evaluation on fault detection in solar panels. Energies, 2021, 14(22): 7770.

[24] KUMAR B, GARG D, SWAMY K, et al. Clean energy production using solar energy resources//PAL D B, JHA J M. Sustainable and Clean Energy Production Technologies, Singapore: Springer, 2022: 269-288.

[25] AKASH S, SATYA S S, JAGADEESH S, et al. Solar cell efficiency improvement techniques. International Journal for Recent Developments in Science and

Technology, 2022, 6(1): 69-77.
[26] ABBASSI A, BEN MEHREZ R, TOUAITI B, et al. Parameterization of photovoltaic solar cell double-diode model based on improved arithmetic optimization algorithm. Optik, 2022, 253: 168600.
[27] LOUZAZNI M, BELMAHDI B, MADHIARASAN M. Modeling and Analysis of the Effect of Current-Voltage in the Solar Cell Dynamic Parameters//The 16th International Conference Interdisciplinarity in Engineering, October. 6-7, 2022, Târgu Mureș, Romania. Cham: Springer, 2023: 696-705.
[28] COTFAS P A, COTFAS D T, BORZA P N, et al. Solar cell capacitance determination based on an RLC resonant circuit. Energies, 2018, 11(3): 672.
[29] OZAKI M, ISHIKURA Y, TRUONG M A, et al. Iodine-rich mixed composition perovskites optimised for tin (iv) oxide transport layers: The influence of halide ion ratio, annealing time, and ambient air aging on solar cell performance. Journal of Materials Chemistry A, 2019, 7(28): 16947-16953.
[30] SHARMA D K, PAREEK K, CHOWDHURY A. Investigation of solar cell degradation using electrochemical impedance spectroscopy. International Journal of Energy Research, 2020, 44(11): 8730-8739.

太阳能电池宽带阻抗谱和同步直流伏安测量系统

肖文波[1,2,3*], 李　傲[2], 吴华明[2], 李勇波[2]

1. 南昌航空大学 科技学院, 江西 九江 332020;
2. 南昌航空大学 光电信息感知技术与仪器江西省重点实验室, 江西 南昌 330063;
3. 南昌航空大学 无损检测技术教育部重点实验室, 江西 南昌 330063

摘　要: 目前, 由于成本、复杂性和准确性等问题, 阻抗谱测量技术在诊断太阳能电池故障方面面临诸多困难。为此, 基于阻抗谱测量原理和太阳能电池模型, 开发了一种精确测量太阳能电池宽带阻抗谱的新型系统, 其由示波器、信号发生器和采样电阻组成。结果表明, 该系统能够同时准确测量频率范围为50 Hz至0.1 MHz的阻抗谱, 并获取直流伏安特性。与Keithley 2450的数据进行比较, 全局相对误差约为6.70%, 证实了其准确性。在四种激励信号(正弦波、方波、三角波和脉冲波)中, 正弦波输入产生了较准确的数据, 与理论数据相比, 均方根误差约为13.301 6, 全局相对误差约为4.25%。提高参考电阻会扩大阻抗谱中的半圆。当参考电阻接近太阳能电池的电阻, 通过减少线路电阻的影响, 可提高测量准确性。由于信噪比较高, 高频段的测量误差低于低频段。

关键词: 太阳能电池; 示波器; 信号发生器; 伏安特性; 阻抗谱

引用格式: XIAO Wenbo, LI Ao, WU Huaming, et al. Construction of a broadband impedance spectrum and synchronous DC voltammetry measurement system for solar cells. Journal of Measurement Science and Instrumentation, 2024, 15(3): 302-307.